Fifth International Symposium on Marine Propulsors
smp'17, Espoo, Finland, June 2017

A Generalised Boundary Element Method to Analyse Marine Current Turbines Hydrodynamics Including Flow Separation and Stall

Francesco Salvatore[1], **Zohreh Sarichloo**[1], **Danilo Calcagni**[1]

[1] Italian Marine Technology Research Institute (CNR-INSEAN), Rome, Italy

ABSTRACT

A computational model for the hydrodynamic analysis of horizontal axis marine current turbines is presented. The methodology is an original extension of a Boundary Integral Equation Method (BIEM) for inviscid flows to describe the flow features that characterize hydrokinetic turbines. To this purpose, semi-analytical trailing wake and viscous-flow correction models are introduced. A validation study is performed by comparing hydrodynamic performance predictions with experimental data on a model turbine with variable pitch blades. The capability of the proposed methodology to correctly describe turbine thrust and power over a full range of operating conditions is demonstrated. Viscosity effects associated to blade flow separation and stall are predicted and thrust and power are comparable with results of blade element methods that are largely used in the design of marine current turbines.

Keywords

Marine Current Turbine, Hydrodynamics, Boundary Element Method, Separated Flow, CFD Validation.

1 INTRODUCTION

Hydrokinetic turbines for the production of marine renewable energy from tidal and ocean currents is a rapidly maturing technology with first utility-scale installations expected to become reality in the next few years. Technology is converging to horizonthal-axis turbines and system layout reflects in many respects solutions that are well proven from the wind energy sector. In most cases the geometry of marine current turbine blades resembles wind rotor blades except for the aspect ratio that is quite smaller to resist hydrodynamic loads in water.

It is then not surprising that the design of hydrokinetic turbines is largely based on Blade Element Methods (BEM) that are extensively used for wind turbines, see *e.g.* Hansen (2008). These methods allow to determine fast and reliable estimates of turbine performance if suitable tuning is applied to overcome important methodology weaknesses (Buhl 2005, Shen et al 2005). Specifically, blade loading is derived by prescribed lift and drag properties of two-dimensional profiles and semi-empirical three-dimensional flow corrections are necessary to account for blade tip effects, blade/hub interaction, number of blades.

In contrast to this, the hydrodynamic design of marine propellers is typically based on boundary element or panel methods that, under limiting inviscid-flow assumptions, provide a consistent representation of the three-dimensional flow around rotors in steady or unsteady flow. In spite of that, few example exist of applications of this type of methods to hydrokinetic turbines, see *e.g.* Baltazar & Falcão de Campos (2009, 2011), Young et al (2010). Results in the literature show the difficulty of boundary element methods to correctly describe the hydrodynamic performance of turbines designed to extract energy from an onset flow. A major difficulty is that turbine blades frequently operate at high angle of attack and viscous-flow separation and stall effects on generated thrust and power are important over a wide range of operating conditions.

Aim of the present work is to describe the development of a boundary element model for the analysis of marine current turbines. To avoid confusion with blade element methods, the terminology Boundary Integral Equation Method (BIEM) is used here. The approach is derived from a BIEM developed for marine propellers and extensively validated, see Salvatore et al (2003, 2011), Pereira et al (2004). The extension to describe hydrokinetic turbine flows is achieved by introducing models for the trailing vorticity pattern and for the viscosity correction of blade loads. The trailing wake geometry is determined by a semi-analytical model with wake pitch alignment consistent with turbine-induced velocity perturbation and an experimental-based expansion law of the streamtube downstream the turbine. Inspired to blade element methods, viscous-flow correction is determined by comparing distributions of blade loads by the inviscid-flow BIEM and lift and drag properties of representative blade sections under flow separation and stall. Polar curves are obtained from available experimental data.

A validation study is addressed by considering experimental data in Bahaj et al (2007) where a detailed characterization of a model marine current turbine with variable pitch blades is presented. Numerical results demonstrate the capability of the proposed methodology to determine reliable predictions of turbine hydrodynamic performance over a full range of operating conditions. In particular, the accuracy of turbine thrust and power predictions is fully comparable with results from well established blade element methods.

2 THEORETICAL MODEL

The computational model proposed here for the hydrodynamic analysis of marine current turbines is based on a Boundary Integral Equation Method (BIEM) that is valid under inviscid flow assumptions. The methodology has been originally developed to study marine propulsors, see *e.g.*, Salvatore et al (2003, 2011), Pereira et al (2004).

Here, the computational model is adapted to describe the peculiarities of marine turbine flows. Specifically, marine propulsors and marine turbines require different modelling approaches to describe trailing vorticity dynamics, and to correct blade loads under flow separation and stall. In this section, the basic BIEM is briefly reviewed and models for trailing vorticity and viscosity effects are described.

Assuming the onset flow is incompressible, irrotational and inviscid, the perturbation velocity $\mathbf{v}$ induced by the turbine may be described by a scalar potential as $\mathbf{v} = \nabla\varphi$, and general mass and momentum equations are dramatically simplified. Mass conservation is recast as the Laplace equation for the perturbation velocity potential, $\nabla^2\varphi = 0$, while the momentum equation reduces to the Bernoulli equation for the pressure p

$$\frac{\partial\varphi}{\partial t} + \frac{1}{2}\|\nabla\varphi + \mathbf{v}_I\| + \frac{p}{\rho} + gz_0 = \frac{1}{2}\|\mathbf{v}_I\|^2 + \frac{p_0}{\rho}, \quad (1)$$

where p_0 is the free-stream reference pressure, and $\mathbf{v}_I = \mathbf{w} + \mathbf{\Omega} \times \mathbf{x}$ is the inflow velocity as seen from an observer fixed with blades rotating at angular velocity $\mathbf{\Omega}$ while $\mathbf{w}$ is the onset flow velocity. In case of uniform inflow aligned to turbine axis x, one has $\mathbf{\Omega} = \Omega\mathbf{e}_x, \mathbf{w} = V\mathbf{e}_x$ with $\mathbf{e}_x$ unit vector along x. Finally, gz_0 is the hydrostatic head term referred to a reference vertical position $z = 0$.

The Laplace equation for φ is solved via a boundary integral formulation where problem unknowns are distributed on the body surface and on its *trailing wake*. By potential flow theory for lifting bodies, the trailing wake denotes a zero-thickness layer where vorticity generated by lifting surfaces is shed into the downstream flow. Through a classical derivation (see, *e.g.*, Morino 1993) the following boundary integral representation for φ at an arbitrary field point $\mathbf{x}$ is obtained

$$\begin{aligned} E(\mathbf{x})\,\varphi(\mathbf{x}) &= \oint_{\mathcal{S}_{B\cup N}} \left(\frac{\partial\varphi}{\partial n}G - \varphi\frac{\partial G}{\partial n}\right) d\mathcal{S}(\mathbf{y}) \\ &- \int_{\mathcal{S}_W} \Delta\varphi\frac{\partial G}{\partial n} d\mathcal{S}(\mathbf{y}) \end{aligned} \quad (2)$$

where $\mathcal{S}_{B\cup N}$ denotes the body surface (turbine nacelle and blades), $\mathcal{S}_W$ is the trailing wake and $\mathbf{n}$ is the unit normal to these surfaces. The symbol Δ in Eq. (2) is used to denote discontinuity of velocity potential across the trailing wake surface, whereas $E(\mathbf{x})$ is a function that makes the same equation to be valid for points $\mathbf{x}$ on the body surface ($E = 1/2$) or inside the fluid domain, $E = 1$. Moreover, quantities $G, \partial G/\partial n$ are unit source and dipoles in the unbounded three-dimensional space and depend only from the mutual position between the collocation point $\mathbf{x}$ and the influencing point $\mathbf{y}$ on the boundary surfaces.

Boundary conditions for the velocity potential are imposed at infinity (vanishing perturbation φ), on solid surfaces (impermeability, $\partial\varphi/\partial n = -\mathbf{v}_I \cdot \mathbf{n}$) and on the trailing wake, where convection of vorticity generated on blades is imposed and a Kutta-Morino condition is used to impose identity between velocity potential difference at blade trailing edge upper and lower sides and $\Delta\varphi$ on the wake.

Equation (2) with $E = 1/2$ and related boundary conditions represents a boundary integral equation whose solution determines φ on the body surface. By discretizing boundaries $\mathcal{S}_{B\cup N}$ and $\mathcal{S}_W$ into surface panels, and enforcing Eq. (2) at centroids of body panels, a linear set of algebraic equations is obtained. The wake surface $\mathcal{S}_W$ can be determined as a part of the solution by a wake-alignment iterative procedure, see Greco et al (2004). A faster and more robust approach is used in the present study as described in Section 2.1.

Once Eq. (2) is numerically solved, the velocity potential and its gradient are known on the body surface and pressure can be evaluated using the Bernoulli Eq. (1). Hydrodynamic loads generated by the turbine are then obtained by integrating pressure and tangential stress τ over the blades surface. In particular, force contribution by a blade element at radius r with span $\mathrm{d}r$ and surface $\mathrm{d}\mathcal{S}$ can be written as

$$\mathrm{d}\mathbf{f}(r) = \mathrm{d}\mathbf{f}_p(r) + \mathrm{d}\mathbf{f}_\tau(r) = \int_{\mathrm{d}\mathcal{S}} (-p\,\mathbf{n} + \tau\,\mathbf{t})\, d\mathcal{S}, \quad (3)$$

where $\mathbf{t}$ is the unit vector tangent to the surface and aligned to the local flow and quantities $\mathbf{f}_p, \mathbf{f}_\tau$ denote, respectively, contributions by normal (pressure) and tangential (friction) stress. Integrating elementary forces on all blades, turbine thrust T and torque Q follow

$$T = \int_{S_B} \mathbf{f} \cdot \mathbf{e}_x\, d\mathcal{S}, \qquad Q = \int_{S_B} (\mathbf{x} \times \mathbf{f}) \cdot \mathbf{e}_x\, d\mathcal{S}. \quad (4)$$

Surface stress τ is not part of the inviscid-flow solution and could be evaluated by a coupled viscous/inviscid model in which BIEM is combined with a boundary-layer model, as described in Salvatore et al (2003). A simplified approach popular in marine propulsors models consists in estimating quantity τ from formulas valid for attached laminar and turbulent flow over a flat plate (Carlton 1994).

$$\begin{aligned} C_F &= 1.328/\sqrt{Re_r} \qquad (Re_r < 10^5) \\ C_F &= 0.075/\left(log_{10}(Re_r) - 2\right)^2 \quad (Re_r \geq 10^5) \end{aligned} \quad (5)$$

where $C_F = \tau/\frac{1}{2}\rho V_I^2(r)$, and $Re_r = c(r)V_I(r)/\nu$ is the Reynolds number defined through local blade chord $c(r)$, local inflow velocity $V_I(r) = [V^2 + (\Omega r)^2]^{1/2}$, and ν denotes water kinematic viscosity. The accuracy of this viscosity correction to hydrodynamic loads by BIEM is typically limited to attached flows on blade sections at low angle of attack. Section 2.2 describes the approach proposed here to cope with a wider range of conditions including flow separation and stall.

2.1 Trailing wake model

In the present study, a semi-analytical model is used to determine the wake surface $\mathcal{S}_W$ in Eq. (2). The wake is defined as a generalised helicoidal surface with distributions of axial pitch and of radial extension that are consistent with the operating mode of hydrokinetic turbines.

For the axial pitch, two regions are considered: the *tip-vortex* region and the *blade wake* extending spanwise at lower radius up to the vortex released at blade root. In the blade wake, trailing vortices are convected downstream with velocity given by the sum of the onset flow speed and of the velocity perturbation induced by the wake itself, $\mathbf{v}_w$. Here, an approximated representation of this velocity field is obtained by evaluating by BIEM its distribution at the rotor plane and imposing a linear variation downstream the rotor plane to match a farfield distribution. A simplified expression for the induced axial velocity follows as

$$v_{x,w} \;=\; (1-\xi_x)\,\frac{\partial\tilde{\varphi}}{\partial x}\Big|_{RP} \;+\; \xi_x\, v_{x,w}\big|_{FF} \qquad (6)$$

where ξ_x is a normalised abscissa with $\xi_x = 0$ at rotor trailing edge and $\xi_x = 1$ at the downstream end of the discretised wake surface. Consistent with Betz theory (Betz 2013), the axial induced velocity at farfield $v_{x,w}|_{FF}$ is twice the intensity at the rotor plane. Symbol $(\tilde{\ })$ denotes wake-induced velocity potential from Eq. (2), and subscript RP refers to the rotor plane axial position.

In the tip-vortex region, Okulov & Sørensen (2010) describe a trailing vortex shedding model with axial velocity given as the average between velocity in the blade wake, here given by Eq. (6), and the unperturbed onset flow velocity V. Thus, denoting by $\phi_{w,0}$ the hydrodynamic pitch associated to the unperturbed flow, one obtains the following expressions for the wake pitch ϕ_w

$$\begin{aligned}
\phi_{w,bla} &= \left(1+\frac{v_{x,w}}{V}\right)\phi_{w,0},\\
\phi_{w,tip} &= \frac{1}{2}\left(\phi_{w,bla}+\phi_{w,0}\right),\\
\phi_w &= \xi_r\phi_{w,tip} \;+\; (1-\xi_r)\phi_{w,bla},
\end{aligned} \qquad (7)$$

where pedices bla and tip denote quantity referred to, respectively, blade wake and tip vortex, and $\xi_r = (r/R)^{C_1}$ is a weight function ($C_1 > 3$, where R is the rotor radius).

Next, the radial expansion of the wake streamtube downstream the rotor plane is determined as

$$r \;=\; R \;+\; r_0\left(1-e^{-\xi_x/C_2}\right) \qquad (8)$$

where constants r_0, C_2 are derived from experimental data describing the wake evolution of hydrokinetic turbines over a range of operating conditions. In the present study, wake flow measurements by Mycek et al (2014) (here referred to as IFREMER rotor) and by Del Frate et al (2016) (SABELLA rotor) have been considered, see Fig. 1. The assumption is that at short distance from the rotor, trailing wake expansion is weakly dependent by the rotor shape and a general trend can be derived from flow measurements.

Combining Eqs. (6) to (8), the generalised helicoidal surface defining the trailing wake $\mathcal{S}_W$ is obtained. In fact, the evaluation of the velocity potential $\tilde{\varphi}$ in Eq. (6) depends on the definition of surface $\mathcal{S}_W$ in Eq. (2) and hence an iterative procedure is required.

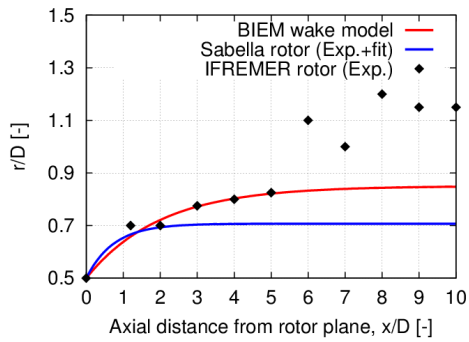

Figure 1: Streamtube radius downstream rotor plane from Eq. (8) and comparative data from experiments.

2.2 Viscous-flow correction model

Assumptions of inviscid, irrotational flow underlying BIEM yield that turbine hydrodynamics is studied by fast numerical solutions of a linear problem with unknowns distributed only on the solid surface of the turbine. Unfortunately, turbine performance is dramatically affected by blade flow separation and stall and hence neglecting viscosity effects may results into completely unreliable predictions of turbine hydrodynamic loads and power output.

A methodology is proposed here to correct blade loads predicted under inviscid-flow assumptions by a procedure that preserves the reduced computing effort typical of BIEM. The idea is to *(i)* identify conditions where blade flow is subject to boundary layer separation and stall and *(ii)* estimate the effect of viscosity on blade loads under such conditions. The BIEM model including this viscous-flow correction is hereafter referred to as BIEM-VFC.

To this purpose, sectional loads along blade span evaluated by BIEM are compared to lift and drag properties of two-dimensional (2D) profiles describing blade sections. Equivalence between operating conditions of three-dimensional rotating blade sections and corresponding 2D profiles is enforced in terms of local Reynolds number Re_r (see Section above) and of the *effective* angle of attack α_e.

Quantity α_e is the angle of attack when wake-induced velocity contributions are accounted for to evaluate the total velocity incoming to blade sections, see Fig. 2, where inflow velocity components and hydrodynamic force components referred to blade section at radius r of a turbine rotating at angular speed Ω are sketched. Axial and tangential induced velocity components, respectively Δu_i and Δv_i, represent three-dimensional flow effects induced by trailing vortices shed by blades. These quantitites are zero in case of 2D flow around a lifting surface of infinite span and the effective and nominal angle of attack α coincide.

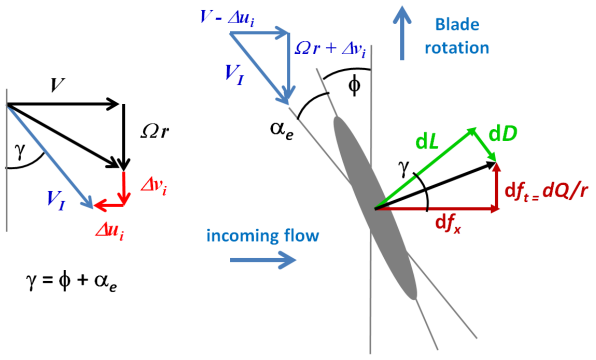

Figure 2: Inflow velocity components and hydrodynamic force components on turbine blade section at radius r.

Lift and drag properties representative of blade section shape and operating conditions (α_e, Re_r) are deduced from 2D foil polar curves, as sketched in Fig. 3. Flow separation occurs when the lift curve departs from linear dependence with incidence α (points labelled as SE+, SE-), while stall occurs when lift drops as α increases in absolute value and drag has an abrupt rise (point ST).

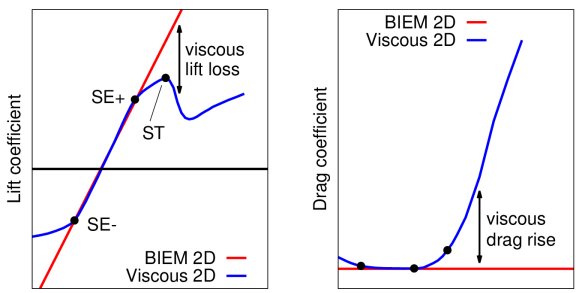

Figure 3: Lift and drag curves of two-dimensional profile: viscous-flow compared with corresponding quasi-inviscid flow.

Inviscid-flow solutions by BIEM determine blade sectional loads that are consistent with linear relationship between lift and angle of attack and, using the flat-plate analogy in Eq. (5) with minimum drag reflecting attached flow conditions (curves in red in Fig. 3). The comparison between sectional lift and drag properties motivates the following definition of factors to correct sectional loads by BIEM to represent both attached and separated flow conditions:

$$\begin{aligned} \mathcal{K}_D(\alpha_e, Re_r) &= \mathrm{d}D_{2D}/\mathrm{d}D_{2D}^{inv} \\ \mathcal{K}_L(\alpha_e, Re_r) &= \mathrm{d}L_{2D}/\mathrm{d}L_{2D}^{inv} \end{aligned} \tag{9}$$

where D_{2D}^{inv} and L_{2D}^{inv} are, respectively, drag and lift per unit length determined under inviscid 2D flow conditions (*i.e.* by BIEM) at angle of attack α_e, while D_{2D} and L_{2D} are profile drag and lift from 2D flow polar curves.

Once quantities $\mathcal{K}_D, \mathcal{K}_L$ are known, blade loads correction is obtained through the following procedure. From the BIEM solution, sectional contributions to axial force $\mathrm{d}f_x$ and tangential force $\mathrm{d}f_t$ are determined from Eq. (3). Next, wake-induced velocity along blade span is determined by taking the gradient of Eq. (2) (with $E = 1$), and the radial distribution of the effective angle of attack $\alpha_e(r)$ is evaluated. Radial distributions of sectional drag and lift $\mathrm{d}D, \mathrm{d}L$ follow by projecting force in direction normal and tangent to the effective inflow, as sketched in Fig. 2, where ϕ is the angular pitch of blade section at radius r.

Separating pressure-induced and friction-induced contributions to force $\mathrm{d}\mathbf{f}$ as defined in Eq. (3), lift and drag contributions are also splitted into pressure-induced and friction-induced terms. Correction factors from Eq. (9), yield

$$\begin{aligned} \mathrm{d}\hat{L}_p &= \mathcal{K}_L \mathrm{d}L_p, & \mathrm{d}\hat{D}_p &= \mathcal{K}_L^2 \mathrm{d}D_p \\ \mathrm{d}\hat{L}_\tau &= \mathcal{K}_D \mathrm{d}L_\tau, & \mathrm{d}\hat{D}_\tau &= \mathcal{K}_D \mathrm{d}D_\tau \end{aligned} \tag{10}$$

where symbol $(\hat{\ })$ labels viscous-flow corrected quantities. While corrections for pressure-induced lift L_p and friction-induced drag D_τ are obvious, the assumption made here is that correction factor for drag $\mathcal{K}_D$ can be used to account for flow separation and stall effects on friction-induced lift L_τ. Pressure-induced drag D_p correction by $\mathcal{K}_L^2$ stems from the approximated relationship between induced drag and lift that is broadly valid for lifting surfaces.

Converting lift and drag back to respectively axial and tangential load components yields quantitity $\mathrm{d}\hat{f}_x$ that integrated along blade span returns blade axial force, while quantity $\mathrm{d}\hat{Q} = \mathrm{d}\hat{f}_t r$ returns blade torque. Summing on all blades, turbine corrected thrust $\hat{T}$ and torque $\hat{Q}$ are obtained (formally, Eq. (4) with $\mathbf{f}$ replaced by $\hat{\mathbf{f}}$).

A full exploitation of the viscosity correction model described above implies that an iterative procedure is enforced to make the potential flow solution consistent with the modified loading on blades. An original approach is considered here in which a correction in the boundary integral representation (2) is introduced following a viscous/inviscid coupling methodology proposed in Morino et al (1999). The validation of this model is underway and numerical applications described in the present study do not include iterations for the viscosity correction.

3 CASE STUDY AND COMPUTATIONAL SET-UP

The capability of the proposed BIEM-VFC computational model to describe marine current turbine performance is investigated through the case study in Bahaj et al (2007). A tri-bladed model turbine designed for research purposes at the University of Southampton (U.K.) was analysed by extensive towing tank and cavitation tunnel tests. Experimental data include turbine performance at different blade pitch settings, with blades rotated about the spanwise axis over a range of 15 degrees.

Main turbine geometry parameters are summarized in Table 1. In the present study, blade pitch settings $\Phi = 20°$ to $30°$ are considered. Model turbine performance measurements describe operating conditions with Tip Speed Ratio, $TSR = \Omega R/V$, up to a maximum value depending on pitch setting (TSR_{max}=11.3 for $\Phi = 20°$ and 5.7 for $\Phi = 30°$).

Rotor diameter, D	800 [mm]
Blades number, Z	3
Pitch angle at 20% span, Φ	$15, 20, 25, 27, 30$ [deg]
Thickn. ratio, 75% span, t/c	0.151
Hub/rotor diameter ratio	0.125
Blade section profile	NACA 63-8xx

Table 1: Turbine geometry parameters (Bahaj et al 2007).

Figure 4 shows the model turbine in the cavitation tunnel and the three-dimensional model used in the present computational study. A simplified geometry is considered for numerical simulations: the nacelle downstream the rotor is shorther than the physical one and no stanchion supporting the turbine is included. The picture on the right side also shows the computational grid built to discretize turbine nacelle and blades surfaces and the wake shed by one blade.

A grid sensitivity study has been conducted (Sarichloo 2017) to determine discretization parameters providing negligible grid refinement effects. As a result, 72 elements along blade chord and 36 elements spanwise (blade and wake), 42 and 54 elements on the nacelle, respectively, in circumferential and longitudinal directions, and 60 elements streamwise per wake revolution are used. The wake surface extends for 10 revolutions.

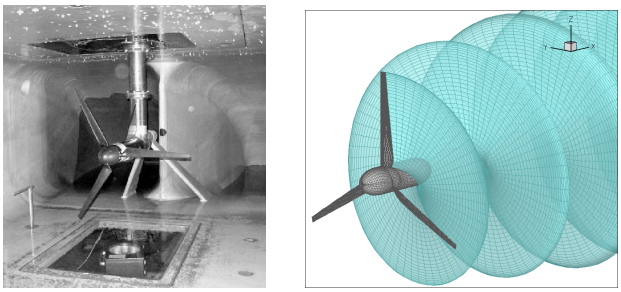

Figure 4: Case study turbine. Left: physical model in the cavitation tunnel (from Bahaj et al 2007). Right: three-dimensional model and computational grid for BIEM analysis.

3.1 Wake geometry

The wake surface has been determined by the trailing wake model described in Section 2.1. Figure 5 depicts the intensity of wake-induced velocity $v_{x,w}$ in Eq. (6) evaluated by BIEM at axial locations corresponding to rotor blade trailing edge and 70% of blade span for different blade pitch settings and over a range of operating conditions corresponding to model tests.

Examples of the resulting trailing wake surface for three values of *TSR* and blade pitch setting $\Phi = 20°$ are shown in Fig. 6. The dependence of wake axial pitch from *TSR* is apparent: trailing vortices are rapidly shed away from the rotor when *TSR* is low, while wake spirals tighten close to the rotor as *TSR* increases. The different pitch between blade wake and tip vortex is also clearly visible.

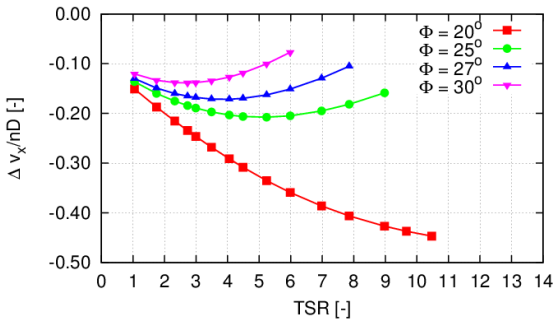

Figure 5: Non-dimensional axial induced velocity at rotor plane and at 70% of blade span. Four pitch settings Φ compared.

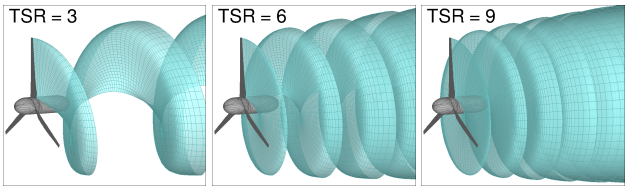

Figure 6: Wake geometry of BIEM model at different operating conditions. From left to right, *TSR* = 3, 6, 9. Case $\Phi = 20°$.

3.2 Viscous flow correction

The impact of viscosity effects on turbine loads is primarily driven by blade-flow parameters like radial distributions of Reynolds number Re_r and angle of attack (AoA). Figures 7 and 8 illustrate the variation of the two quantities over the turbine blade span for *TSR* values corresponding to model tests. In particular, Fig. 7 shows that Re_r approximately varies between $1 \cdot 10^5$ and $3.5 \cdot 10^5$ over most of the operating range. This result depends only on operating parameters V, Ω and is not affected by changes of blade pitch setting.

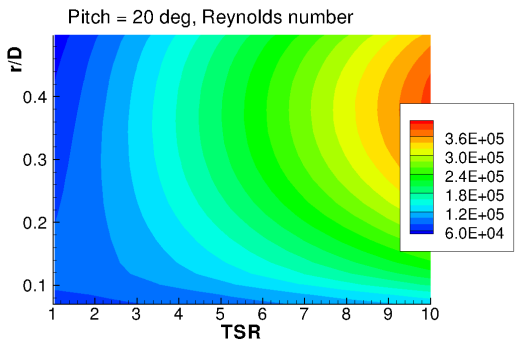

Figure 7: Reynolds number Re_r as a function of radius r and of turbine operating condition (*TSR*).

Figure 8 maps the effective angle of attack α_e as evaluated by BIEM for the lowest and highest pitch settings addressed here, $\Phi = 20°, 30°$. Case $\Phi = 20°$ shows blade sections mostly operating in the range $-5° < \alpha_e < 25°$ with higher values only at *TSR* < 2. As expected, at higher pitch setting angle, the α_e range shifts to lower values.

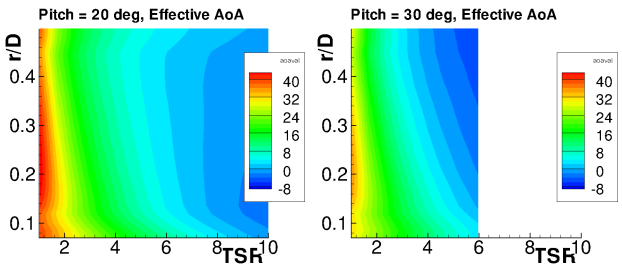

Figure 8: Effective angle of attack α_e as a function of radius r and of turbine operating condition (*TSR*). Pitch setting $\Phi = 20°$ (left) and $\Phi = 30°$ (right).

Once Reynolds number and angle of attack range is established, blade loads correction factors from Eqs. (9) are evaluated. Molland et al (2004) provide lift and drag curves of the NACA 63-815 (15% thick) foil as representative of turbine blade sections, whose thickness ratio varies from 0.176 at 50% of span to 0.126 at tip. It should be noted that chord-based Reynolds number in 2D foil model tests is higher ($Re = 8 \cdot 10^5$) than values mapped in Fig. 7. Similarly, these model tests describe an angle of attack range ($-10° < \alpha < 20°$) that only partially covers the range shown in Fig. 8. High-AoA lift and drag values are obtained here by considering experimental data for the NACA 0015 profile (Sheldahl & Klimas 1981). The assumption is that high-incidence hydrodynamic loads are not sensitive to profile shape details. A polynomial fit is used to merge NACA 63-815 and high-AoA NACA 0015 data at angle of attack between stall and 30 degrees. Resulting lift and drag curves are plotted in Fig. 9, where experimental data for the NACA 63-815 foil in Molland et al (2004), high-AoA NACA 0015 data from Sheldahl & Klimas (1981) are also presented. It may be noted that stall conditions occur at about 10-15 degrees and hence turbine blades undergo flow separation and stall over a significative range of operating conditions of interest in the present study.

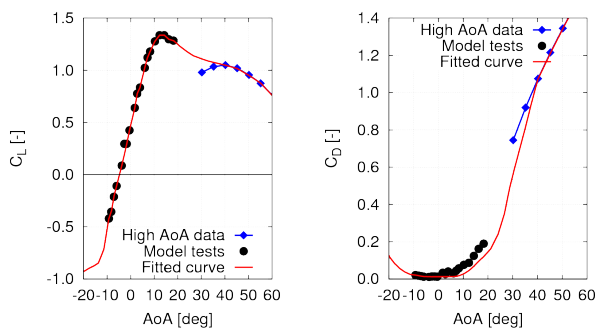

Figure 9: NACA 63-815 2D foil: lift (left) and drag (right) coefficients used for the viscous-flow correction of BIEM.

Lift and drag properties in Fig. 9 are used to feed the viscous-flow correction model described in Section 2.2. In particular, quantities D_{2D}, L_{2D} as function of parameters α_e, Re_r are estimated and correction factors $\mathcal{K}_D, \mathcal{K}_L$ are obtained by Eq. (9). Contour maps in Fig. 10 describe results for two pitch settings, $\Phi = 20°, 30°$. In case $\Phi = 20°$, viscosity effects on blade section lift and drag are negligible at *TSR* of about 3.5-4 and higher, which corresponds to non-separated flow conditions at AoA below 8-10 degrees (cfr. Fig. 9 and left Fig. 8). At lower *TSR* , lift correction factor gradually decreases to about 0.3 (lift loss under stall) while drag correction factor suddenly increases to values of 30 and more (drag crisis). Consistent with sectional angle of attack values commented above, higher pitch settings (bottom Fig. 10) limit flow separation and stall effects to lower values of *TSR* . The impact of this on turbine performance is the subject of results shown in the next section.

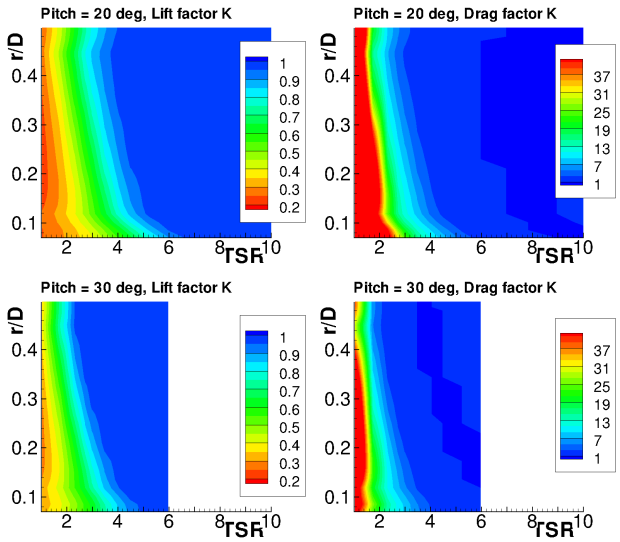

Figure 10: Correction factors for radial contributions to lift (left) and drag (right) as a function of radius r and of of operating condition (*TSR*). Pitch setting $\Phi = 20°$ (top) and $\Phi = 30°$ (bottom).

4 NUMERICAL RESULTS VALIDATION

Turbine performance predictions by BIEM and BIEM-VFC models are compared with model test measurements from Bahaj et al (2007) and with available numerical results from the Literature.

For a turbine having radius R, swept area $A = \pi R^2$, rotating at angular speed $\Omega = 2\pi n$ in a current with nominal freestream velocity V, performance is described through thrust, torque and power coefficients, respectively C_T, C_Q, C_P, defined as

$$C_T = \frac{T}{\frac{1}{2}\rho A V^2}, \qquad C_Q = \frac{Q}{\frac{1}{2}\rho A V^2 R},$$
$$C_P = \frac{Q\,\Omega}{\frac{1}{2}\rho A V^3} = C_Q \cdot \mathrm{TSR}$$

and $P = Q\Omega$ is the power generated by the turbine.

Figure 11 shows results of thrust, torque and power coefficients for the four pitch settings from 20 to 30 degrees. For the sake of precision, Bahaj et al (2007) presents thrust and power coefficients only. Here, also torque coefficient is presented because this quantity provides a direct indication

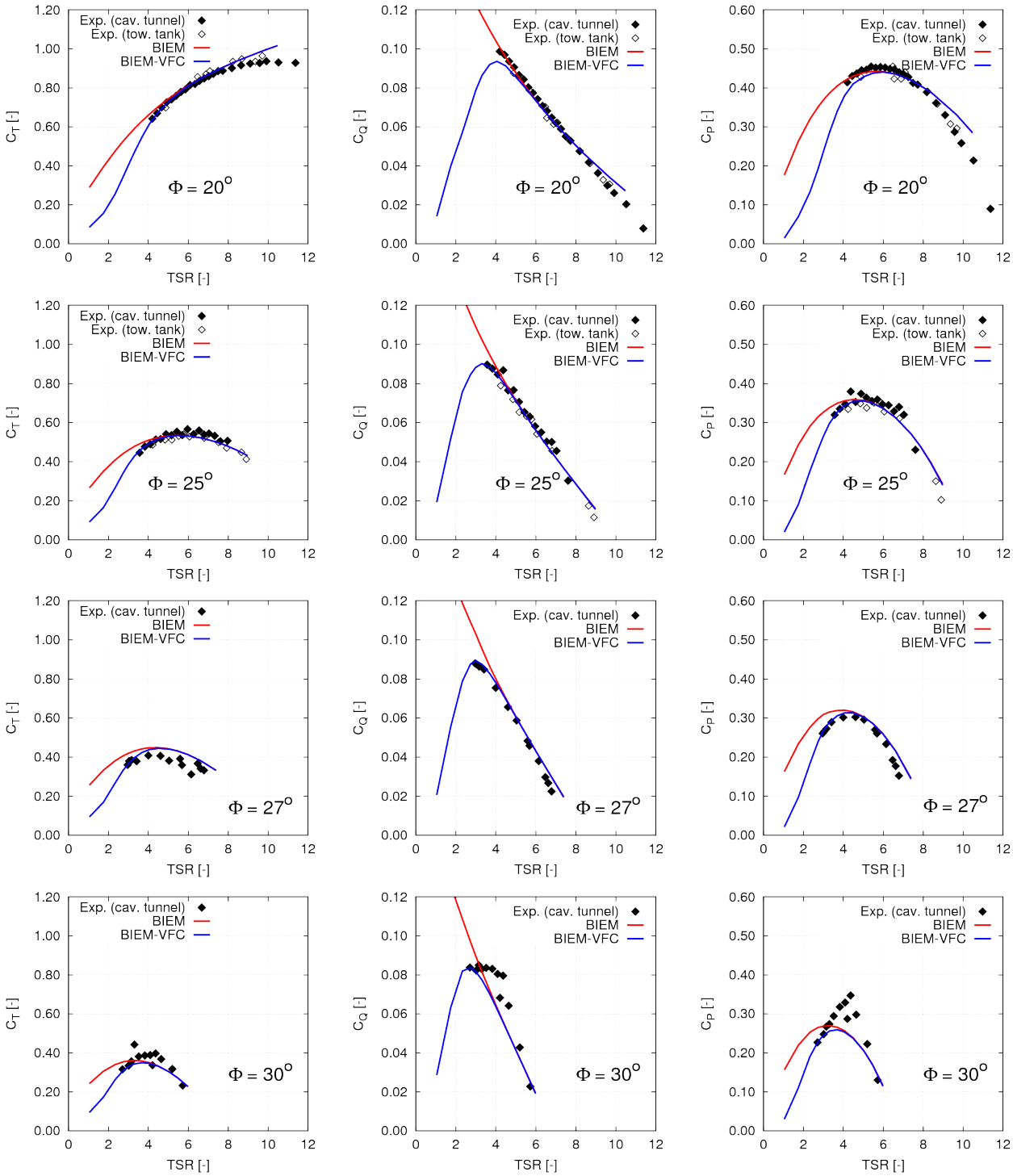

Figure 11: Turbine performance predictions by BIEM and BIEM-VFC compared to experimental data (Bahaj et al 2007). From left to right: thrust, torque, power coefficients. Pitch settings: from top to bottom $\Phi = 20°, 25°, 27°, 30°$.

of the accuracy of blade tangential forces evaluated by the numerical model, while power coefficient is simply derived by it as $C_P = C_Q\ TSR$. Model test results (towing tank and cavitation tunnel data) are in good agreement with numerical predictions by the BIEM-VFC model over the whole range of operating conditions. In contrast to this, plain BIEM model with no viscous-flow correction provides accurate results only at *TSR* higher than the maximum power coefficient is achieved. As discussed above, the high-*TSR* range is characterised by blade flow globally attached and viscosity effects are not dominant. At low *TSR* , flow separation and stall determine thrust, torque and power losses that are completely missed by the plain BIEM. The capability of the VFC model to pro-

vide a physically-consistent correction is apparent for both C_T, C_Q, C_P at all pitch settings with the exception of case $\Phi = 30°$, where C_Q and correspondingly C_P are underestimated for $3 < TSR < 5$. Unfortunately, experimental data do not give information at very low *TSR* where deep-stall conditions are expected. The trend of numerical results by the BIEM-VFC model is qualitatively consistent with literature results describing similar case studies.

Observed discrepancies at $\Phi = 30°$ are commented further by considering Fig. 12, where the effect of blade pitch setting Φ on turbine performance is analysed. To this purpose, four performance indicators are identified: maximum value of thrust coefficient $C_{T_{max}}$, maximum value of power coefficient $C_{P_{max}}$, and corresponding values of *TSR* where maxima are established. Results from model test fits from Bahaj et al (2007) are compared to numerical predictions by BIEM-VFC. Predicted $C_{T_{max}}$ and the corresponding *TSR* fairly reproduce the trend observed in experiments. Same comments can be made for the maximum power except for case $\Phi = 30°$, where predicted $C_{P_{max}}$ is some 20% lower than measurements. Similarly, cases at the highest Φ show that *TSR* where maximum power is generated is slightly underpredicted by BIEM-VFC.

Main weakness of the present approach is that viscosity correction applies only to blade loads and not to the potential flow solution as a whole. In particular, the intensity of blade shed vorticity and tip-vortex is not corrected for viscosity-induced lift loss under flow separation and stall. Such a limitation of the present model is not expected to be the reason of different predicted and measured power in the medium/high *TSR* range, where no VFC-based correction applies, see Fig. 10. In fact, a close view of data for cases at high Φ highlights a peculiar trend of measured $C_{T_{max}}$ and $C_{P_{max}}$ that could be explained with complex blade flow phenomena during model tests that are beyond limits of the present computational model.

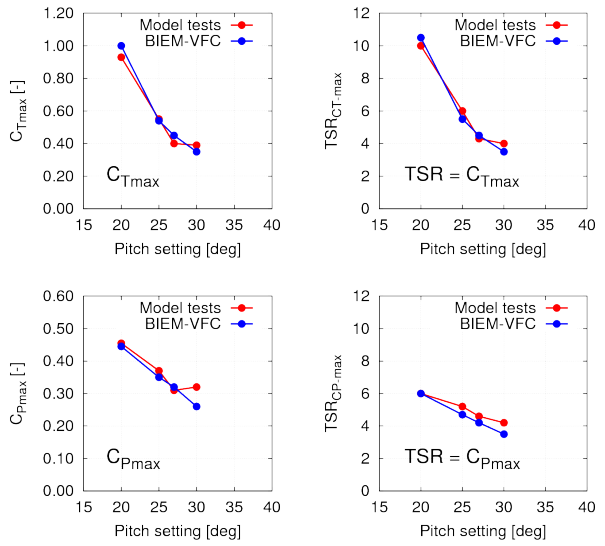

Figure 12: Effect of pitch setting Φ: from top to bottom, left to right, $C_{T_{max}}, C_{P_{max}}$ and corresponding *TSR* values.

Finally, results from the present study are compared in Fig. 13 with data from the literature obtained using different computational models. Two sets of data are selected here for comparison with the BIEM-VFC model: Bahaj et al (2007) present results by two solvers based on Blade Element Method (BEM), a very popular approach for applications to marine turbines (not to mention wind turbines). Next, Baltazar & Falcão de Campos (2009) represents one among few examples in which BIEM is applied to marine turbines. Cited references provide data from BEM for blade pitch settings $\Phi = 20°, 25°, 27°$, while BIEM data address blade pitch settings $\Phi = 20°, 25°$ only. No comparative data are available for the case $\Phi = 30°$.

Considering thrust coefficient, results from BEM solvers GH-Tidal and SERG-Tidal show an accuracy with respect to model test results (Bahaj et al 2007) that is broadly comparable to BIEM-VFC. In details, predictions by BIEM-VFC and GH-Tidal are closer to experiments than SERG-Tidal for pitch settings $\Phi = 20°, 25°$, while the opposite holds for $\Phi = 27°$. Maybe, more interesting is to observe that while BIEM-VFC and SERG-Tidal show a comparable accuracy for power predictions, results by solver GH-Tidal are largely overestimated for all the pitch setting cases. Finally, both thrust and power by the BIEM in Baltazar & Falcão de Campos (2009) is underestimated for both pitch setting cases addressed.

CONCLUSIONS

A computational hydrodynamics model for marine current turbines has been described, and results of a validation study have been presented and discussed. The methodology is based on a Boundary Integral Equation Model (BIEM) for inviscid flows. In order to correctly describe the flowfield around a turbine extracting power from the fluid, a suitable trailing wake model has been introduced. Moreover, a viscous-flow correction (VFC) model has been derived to determine blade thrust and torque losses under conditions of flow separation and stall. Viscosity-induced effects are derived by a semi-empirical approach in which inviscid-flow blade loads by BIEM are corrected on the basis of lift and drag properties of 2D foils describing blade sections under equivalent 3D flow conditions, where equivalence is set forth in terms of the effective angle of attack.

Numerical predictions by BIEM-VFC have been validated through comparisons with experimental data. Results of this study reveal the capability of the proposed methodology to correctly describe turbine performance over a full range of operating conditions. Specifically, accurate predictions of turbine thrust, torque and power are obtained at medium/high Tip Speed Ratio (*TSR*) regimes, when blade flow is globally attached, but also at relatively low *TSR* , where blade flow separation and stall determine thrust loss and drag crisis. Reliable predictions of turbine performance are obtained for blade pitch setting variations over 15 degrees, including design and off-design conditions. In particular, trends describing the relationships between blade pitch setting and turbine performance (thrust,

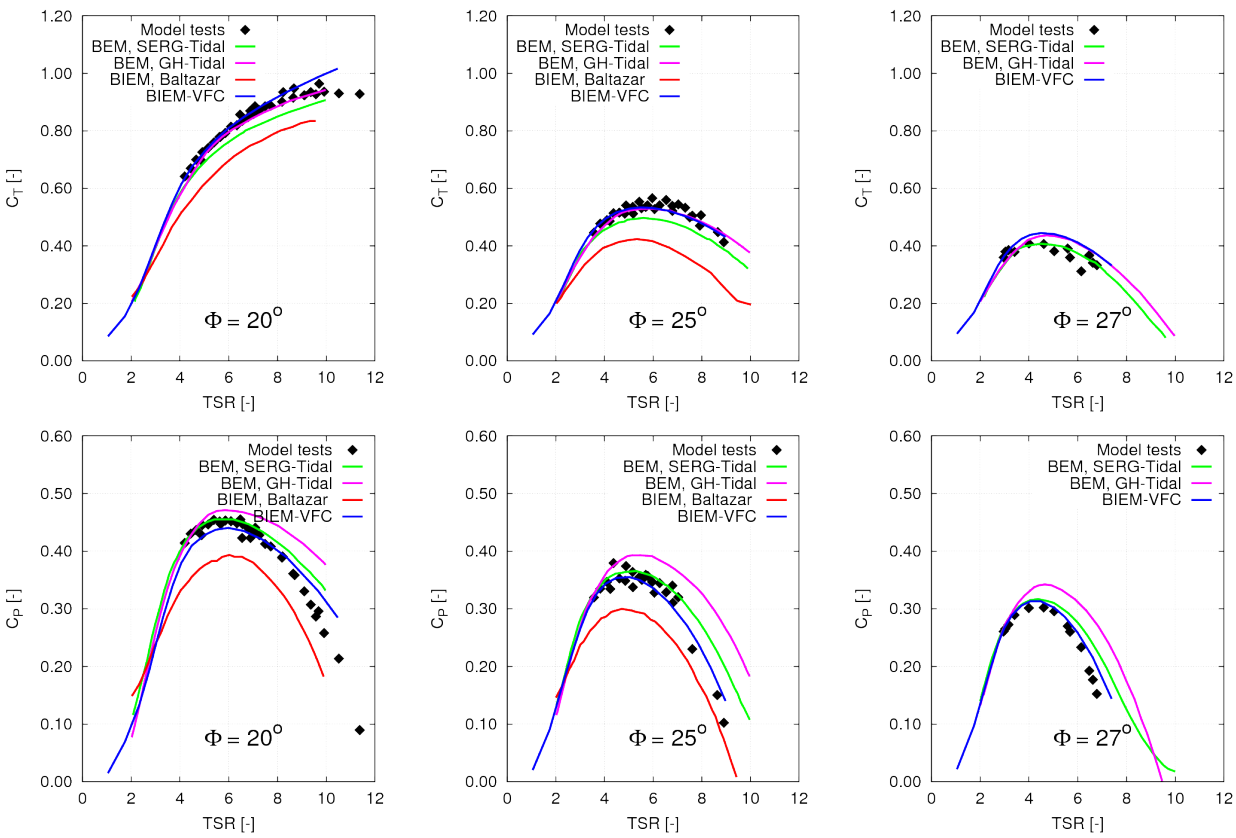

Figure 13: Turbine performance predictions by BIEM-VFC compared to results from the literature: thrust (top) and power (bottom).

power and corresponding *TSR*) observed during experiments are fairly reproduced in numerical results. Unfortunately, benchmark experimental data do not allow to extend the validation study to very low tip speed ratio regimes.

Results by BIEM-VFC have been also compared with numerical results from the literature. A key finding is that proposed model accuracy is fully comparable with Blade Element Methods that are routinely used for the analysis and design of marine as well as wind turbines. Such a result is particularly important in that the present methodology based on BIEM provides a physically consistent description of the three-dimensional flow around a turbine in arbitrary onset flow, while Blade Element Methods rely on taylored, case-dependent corrections for blade tip effects, for blade/hub interaction, number of blades. Well known limitations of blade element methods to analyse non-uniform flow conditions as well as to study turbine cavitation are also overcome through the more general description of turbine flow obtained by a BIEM approach.

Further validation studies focused to investigate the capability of the BIEM-VFC model to describe turbine performance at low *TSR* is the subject of ongoing activity. Main weakeness of the present approach is that viscosity correction applies only to blade loads and not on the potential flow solution as a whole. The implementation of an iterative procedure to achieve blade pressure distribution and tip vortex intensity fully consistent with viscosity correction of blade loads is underway. BIEM-VFC model improvements also address the inclusion of Reynolds number effects in the evaluation of viscous flow correction factors. Following a consolidated approach in Blade Element Methods, the X-Foil solver (Drela 1989) can be used to determine lift and drag properties of blade sections over a Reynolds number range representative of blade flow. The same approach allows to include the effect of section thickness and camber variations along blade span on viscosity correction.

ACKNOWLEDGEMENTS

The work described has been funded under the CNR-INSEAN Project ULYSSES (*Underpinning LaboratorY for Studies on Sea Energy Systems*).

REFERENCES

Bahaj, A.S., Molland, A.F., Chaplin, J.R., Batten, W.M.J. (2007). 'Power and thrust measurements of marine current turbines under various hydrodynamic flow conditions in a cavitation tunnel and a towing tank.' Renewable Energy, **32**, pp. 407–426.

Baltazar, J., Falcão de Campos, J.A.C. (2009). 'Unsteady Analysis of a Horizontal Axis Marine Current Turbine in Yawed Inflow Conditions With a Panel Method.' First International Symposium on Marine Propulsors, Trondheim, Norway, June 2009.

Baltazar, Machado, J., Falcão de Campos, J.A.C. (2011). 'Hydrodynamic design and analysis of horizontal axis marine current turbines with lifting line and panel methods.' ASME 30th Int. Conference on Ocean, Offshore and Arctic Engineering, pp. 453-465.

Betz, A. (2013). 'The Maximum of the Theoretically Possible Exploitation of Wind by Means of a Wind Motor.' Wind Engineering, **37**(4), pp. 441-446. (Translation by Hamann et al. of original paper published in 1920 by the author in German).

Buhl, M.L.Jr. (2005). 'A New Empirical Relationship between Thrust Coefficient and Induction Factor for the Turbulent Windmill State.' Technical Report NREL/TP-500-36834, August 2005.

Carlton, J.S. (1994). Marine Propellers and Propulsion. Butterworth–Heinemann, Oxford, UK, First Edition.

Del Frate, C., Di Felice, F., Alves Pereira, F., Romano, G.P., Dhomé, D., Allo, J.–C. (2016). 'Experimental Investigation of the turbulent flow behind a horizontal axis tidal turbine.' Progress in renewable Energies Offshore, Proceedings of RENEW 2016 2nd International Conference on Renewable Energies Offshore, Lisbon, Portugal.

Drela, M. (1989). 'XFOIL: An Analysis and Design System for Low Reynolds Number Airfoils.' In: Low Reynolds Number Aerodynamics. Proceedings of the Conference Notre Dame, Indiana, USA, 5-7 June 1989. Lecture Notes in Engineering, Bd. 54. Berlin, Heidelberg: Springer 1989, pp. 1–12.

Greco, L., Salvatore, F., Di Felice, F. (2004). 'Validation of a Quasi–potential Flow Model for the Analysis of Marine Propellers Wake.' Twenty-fifth ONR Symposium on Naval Hydrodynamics, St. John's, Newfoundland, Canada.

Hansen, M. O. L. (2008). Aerodynamics of Wind Turbines. Earthscan, London, U.K., Second Edition, 2008.

Mycek, P., Gaurier, B., Germain, G., Pinon, G., Rivoalen, E. (2014). 'Experimental study of the turbulence intensity effects on marine current turbines behaviour. Part I: One single turbine.' Renewable Energy, **66**, pp. 729-746.

Molland, A.F., Bahaj, A.S., Chaplin, J.R., Batten, W.M.J. (2004). 'Measurements and predictions of forces, pressures and cavitation on 2D sections suitable for marine current turbines.' Journal of Engineering for the Maritime Environment, **218**(2), pp. 127-138.

Morino, L. (1993). 'Boundary Integral Equations in Aerodynamics.' Applied Mechanics Reviews **46**(8), pp. 445-466.

Morino, L., Salvatore, F., Gennaretti, M. (1999). 'A New Velocity Decomposition for Viscous Flows: Lighthills Equivalent-Source Method Revisited,' Computer Methods in Applied Mechanics and Engineering **173**(3-4), pp. 317-336.

Okulov, V.L. & Sørensen, J.N. (2010). 'Maximum efficiency of wind turbine rotors using Joukowsky and Betz approaches.' Journal of Fluid Mechanics, **649**, pp. 497-508.

Pereira, F., Salvatore, F., Di Felice, F. (2004). 'Measurement and Modelling of Propeller Cavitation in Uniform Inflow.' Journal of Fluids Engineering, **126**, pp. 671-679.

Salvatore, F., Testa, C., Greco, L. (2003). 'A Viscous/Inviscid Coupled Formulation for Unsteady Sheet Cavitation Modelling of Marine Propellers.' CAV 2003 Symposium, Osaka, Japan, 2003.

Salvatore, F. Greco, L., Calcagni, D. (2011). 'Computational analysis of marine propeller performance and cavitation by using an inviscid-flow BEM model.' Second Int. Symposium on Marine Propulsion, Hamburg, Germany, June 2011.

Sarichloo, Z. (2017). Computational model and experimental verification of marine turbine hydrodynamic performance. Ms Thesis, Faculty of Civil and Industrial Engineering, University "La Sapienza," Rome (in Italian).

Sheldahl, R.E. & Klimas, P.C. (1981). 'Aerodynamic Characteristics of Seven Symmetrical Airfoil Sections Through 180-Deg. Angle of Attack for Use in Aerodynamic Analysis of Vertical Axis Wind Turbines.' Report SAND80-2114, SANDIA, Albuquerque, NM, USA.

Shen, W. Z., Mikkelsen, R., Sœrensen, J. N., Bak, C. (2005). 'Tip Loss Corrections for Wind Turbine Computations.' Wind Energy, **8**, pp. 457-475.

Young, Y.L., Motley, M.R., Yeung, R.W. (2010). 'Three-Dimensional Numerical Modeling of the Transient Fluid-Structural Interaction Response of Tidal Turbines.' Journal of Offshore Mechanics and Arctic Engineering, **132**, pp. 1-12.

DISCUSSION

Question from José Falcão de Campos, IST, Lisbon, Portugal

The authors should be congratulated for their work on the application of the Boundary Element Method to marine current turbines, in particular the effect of aligning the wake. The corrections for lift and drag are based on the effective angle of attack and it would be interesting to investigate how these viscous corrections could be coupled to the determination of the effective angle of attack through the induced velocities in the method. This is one of the features of the Blade Element Momentum Theory which makes it quite adequate to predict the power and thrust characteristics when there is flow separation and stall.

Authors' closure

The authors are grateful to Prof. Falcão de Campos for kind comments and for putting a question that highlights an aspect of primary importance in the proposed methodology. Specifically, two algorithms have been derived to determine (*i*) a trailing wake geometry consistent with turbine-induced velocity perturbations, and (*ii*) a viscosity correction model (VFC) to account for flow separation and stall on blade sectional loads evaluated by BIEM under inviscid flow conditions. It is apparent that the two aspects are interdependent. However, in its present version, the viscous–flow correction is used only to provide an *a posteriori* modification of blade sectional loads and hence the modified load (and circulation) distribution along blade span has no impact on the calculation of the wake geometry and of the effective angle of attack. The generalization of the methodology is the subject of work underway. A direct relationship between axial and tangential force contributions by a blade element at radius r (respectively, $\mathrm{d}f_x, \mathrm{d}f_t$) and turbine-induced velocity perturbation can be formally obtained from momentum theory

$$\begin{aligned} \mathrm{d}f_x(r) &= 4\pi\rho V^2 r \mathrm{d}r\, a(r)\,[1-a(r)] \\ \mathrm{d}f_t(r) &= 4\pi\rho V \Omega r^2 \mathrm{d}r\, a'(r)\,[1-a(r)] \end{aligned}$$

where $a = 1 - V'/V$, $a' = \omega/2\Omega$ are induction factors with V' and ω denoting, respectively, the axial and angular velocity induced by rotor blades at radius r just downstream the turbine. Equations above are based on limiting assumptions, in particular quantities are averaged over a turbine revolution and the number of blades cannot be accounted for. Nonetheless, if blade sectional loads from BIEM-VFC are used in the left–hand side of these equations, expressions for axial and tangential induced velocity components consistent with viscous–flow correction can be determined and used to update the trailing wake geometry following the procedure in Section 2.1. An iterative, coupled trailing-wake alignment/viscous-flow correction algorithm based on this approach will be discussed in a forecoming paper.

An alternative, more general approach to address the problem can be derived on the basis of a viscous/inviscid coupling general formulation, as mentioned in Section 2.2. This is also the subject of work underway.